BIOCHEMISTRY
including biophysical chemistry & molecular biology

Article

pubs.acs.org/biochemistry

Binding of Copper and Silver to Single-Site Variants of Peptidylglycine Monooxygenase Reveals the Structure and Chemistry of the Individual Metal Centers

Shefali Chauhan, Chelsey D. Kline, Mary Mayfield, and Ninian J. Blackburn*

Institute of Environmental Health, Oregon Health and Sciences University, 3181 Southwest Sam Jackson Park Road, Portland, Oregon 97239-3098, United States

Supporting Information

ABSTRACT: Peptidylglycine monooxygenase (PHM) catalyzes the final step in the biosynthesis of amidated peptides that serve as important signaling molecules in numerous endocrine pathways. The catalytic mechanism has attracted much attention because of a number of unique attributes, including the presence of a pair of uncoupled copper centers separated by 11 Å (termed CuH and CuM), an unusual Cu(I)SMet interaction at the oxygen binding M-site, and the postulated Cu(II)−superoxo intermediate. Understanding the mechanism requires determining the catalytic roles of the individual copper centers and how they change during catalysis, a task made more difficult by the overlapping spectral signals from each copper center in the wild-type (WT) protein. To aid in this effort, we constructed and characterized two PHM variants that bound metal at only one site. The H242A variant bound copper at the H-center, while the H107AH108A double mutant bound copper at the M-center; both mutants were devoid of catalytic activity. Oxidized Cu(II) forms showed electron paramagnetic resonance and extended X-ray absorption fine structure (EXAFS) spectra consistent with their previously determined Cu(II)His_3O and Cu(II)His_2O_2 ligand sets for the H- and M-centers, respectively. Cu(I) forms, on the other hand, showed unique chemistry. The M-center bound two histidines and a methionine at all pHs, while the H-center was two-coordinate at neutral pH but coordinated a new methionine S ligand at low pH. Fourier transform infrared studies confirmed and extended previous assignments of CO binding and showed unambiguously that the 2092 cm^{-1} absorbing species observed in the WT and many variant forms is an M-site Cu(I)−CO adduct. Silver binding was also investigated. When H107AH108A and M109I (a WT analogue with both sites intact) were incubated with excess $AgNO_3$, each variant bound a single Ag(I) ion, from which it was inferred that Ag(I) binds selectively at the M-center with little or no affinity for the H-center. EXAFS at the Ag K-edge established a strong degree of similarity between the ligand sets of Cu and Ag bound at the M-center. These studies validate previous spectral assignments and provide new insights into the detailed chemistry of each metal site.

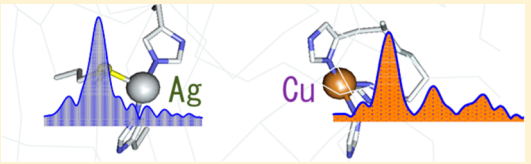

Peptidylglycine monooxygenase catalyzes the final step in the biosynthesis of amidated peptides that serve as important signaling molecules in numerous endocrine pathways.[1] Specifically, the enzyme hydroxylates the α-C atom of the glycine-extended C-terminus of the propeptide in a reaction involving the transfer of four electrons to O_2, two from the C−H bond and two from an external reductant. To conduct this conversion, the enzyme stores the external electrons on a pair of copper atoms that are termed CuH and CuM [also denoted H-site and M-site, respectively (Figure 1)] that are reduced to the Cu(I) state by an external reductant, which is ascorbate under physiological conditions. During turnover, oxygen is believed to bind to Cu(I) at the M-center where it forms a Cu(II)−superoxo species. This activated intermediate then abstracts a H-atom from the α-CH entity of the nearby substrate to form peroxide and a substrate radical. O−O bond cleavage coupled to radical rebound generates a hydroxylated product and a high-valent species [Cu(III)−oxo or Cu(II)−$O^{\bullet-}$] that is reduced to the resting enzyme by a second electron transfer from H to M.

This mechanism has attracted much attention because of a number of unique attributes, many of which have been revealed by crystallography (Figure 1).[2−6] First, the copper centers are 11 Å apart, separated by a solvent-filled cleft in the protein that imposes restrictions on intrasite electron transfer.[7−10] It has been proposed that the physical separation prevents the second electron from being transferred until after the enzyme has committed to catalysis, thereby harnessing the strong electrophilic reactivity of the Cu(II)−superoxo entity.[11,12] Second, the coordination chemistry at each copper is unusual. The M-site is coordinated by H242, H244, and a weak interaction with the thioether of M314,[13−15] which nevertheless plays a critical role in catalysis, because mutation to His, Cys, or Asp results in an ∼95% loss of activity.[16,17] The H-site is bound by three coordinating His residues, H107, H108, and H172,[13,18] mutation of any one of which also eliminates >95% of the catalytic activity. The H-site undergoes an unusual conforma-

Received: November 12, 2013
Revised: January 25, 2014
Published: January 28, 2014

   dx.doi.org/10.1021/bi4015264 | *Biochemistry* 2014, 53, 1069−1080

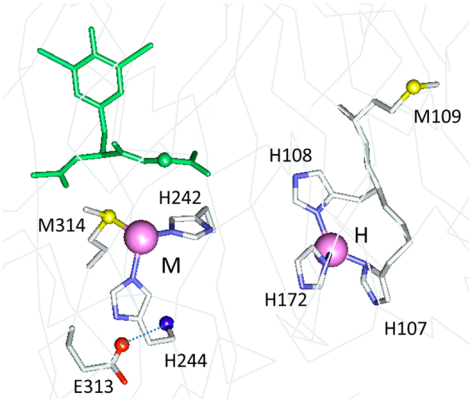

Figure 1. Structure of the PHM active site taken from Protein Data Bank entry 1OPM. This figure shows the H-site coordinated to the Nδ atom of H107, H108, and Nε of H172, and the oxygen binding (catalytic) M-site coordinated to Nε of H242 and H244 and the thiother S of M314. The side chain of the conserved E313 is shown forming an H-bond to the main chain amide nitrogen of H244. The bound substrate (diiodotyrosylglycine) is colored green.

tional change at low pH in which a Met residue (part of a $H^{107}H^{108}M^{109}$ triad) coordinates to the copper and shuts off activity.[19] Furthermore, unlike similar sites in other copper proteins, H does not appear to bind exogenous ligands.[2]

Understanding the individual roles of the electron transfer (H) and oxygen-activating (M) centers is key to unraveling the overall catalytic mechanism. Much of the relevant chemistry, including the template for the binding of oxygen at CuM and the state of CuH immediately prior to ET, occurs in the Cu(I) state that is opaque to many traditional spectroscopic methods because of its d^{10} configuration. Available insight into the structure and reactivity of the Cu(I) forms of PHM and its variants has been derived from X-ray absorption spectroscopy, the one spectroscopic technique that can inform on the Cu(I) state,[13,14,16−20] but the analysis gives only a structural perspective averaged over both copper centers. It is clearly important to obtain site-specific structure−reactivity data for the H- and M-centers individually, to assess the detailed role of each in the overall catalytic process.

We have constructed and characterized two PHM variants that when metalated bind copper and silver at only a single center. The H242A variant is an M-site deletion mutant that removes one of the two histidines necessary for tight binding of copper to the M-site. In previous work,[19] we showed that a similar deletion of one of three histidines at the H-site was insufficient to abrogate copper binding at this site. Accordingly, we constructed double mutant H107AH108A in which removal of two of three histidines now prevents metal binding at the H-center. Here we present a detailed study of each of these single-site variants, in which we show that they do indeed report the individual chemistry and spectroscopy of each site.

MATERIALS AND METHODS

Buffers and ascorbate were obtained from Sigma-Aldrich at a minimal purity of 99%. Beef liver catalase was acquired from Roche. Substrates Ac-Tyr-Val-Gly (Ac-YVG) and dansyl-Tyr-Val-Gly (dansyl-YVG) were purchased from Peptide International and American Peptide Co., respectively.

Construction of Mutants. All variants were constructed using the PHM catalytic core sequence (PHMcc) comprised of residues 42−356. The H107AH108A variant was constructed as previously reported.[20,21] H107AH108A was individually introduced into pBS.ΔProPHM382s (obtained as a gift from B. A. Eipper and R. E. Mains) using splicing by overlap extension (SOEing).[22] Sense and antisense oligonucleotide primers (Table S1 of the Supporting Information) encoding ∼20 bases downstream and upstream of the mutation were used for site-directed mutagenesis and paired with primers upstream and downstream of two restriction enzyme sites, ClaI and XbaI. Polymerase chain reaction (PCR) products were purified on agarose gels. Final PCR products were extracted with phenol and chloroform, digested using restriction enzymes (NEB), fractionated on agarose gels, purified via a Qiagen PCR kit, and then ligated into the pCIS.2CXXNH expression vector (also a gift from B. A. Eipper and R. E. Mains). Sequence analysis was performed on mutant clones, and Qiagen midi prep was used to ensure 20 μg/20 μL of recombinant DNA for transfection.

Screening PHMcc Single-Site Mutants. CHO DG44 cells were transfected with the recombinant DNA using Lipofectamine 2000 (Invitrogen). The transfected cells were subsequently selected for *Dhfr* cell lines in α-minimum Eagle's medium containing 10% dialyzed fetal bovine serum.[21,23] Only those cells that retained the *Dhfr* gene (colocated with PHM on the plasmid) were capable of growth under these conditions. Monoclonal cell lines were created by serial dilution into 96-well plates, to select for wells that contained single-cell colonies. These were passed individually into a fresh 96-well plate, grown to confluence, and screened via Western blotting for PHMcc production under similar conditions. The strongest producers were inoculated into a Hollow Fiber Bioreactor with a MWCO of 5000 (Fibercell Systems, Inc.).

Western Blot Analysis. CHO DG44 cells were incubated in DMEM/F12 medium containing 0.5% Fetal Clone II (FCII, Fisher) for at least 24 h before a sample was collected. It was then mixed with SDS and heated for 5 min at 100 °C. Each sample was separated by 8 to 25% SDS−PAGE and then transferred to an Immobilon P membrane (Millipore) using the PhastSystem (Applied Biosciences). PHM proteins were visualized using rabbit antibody 246 [rPAM(116−131)][24] diluted 1:1500 and secondary antibody anti-rabbit IgG (Sigma) diluted 1:1000, followed by an AP Conjugate Substrate kit (Bio-Rad Laboratories).

PHMcc Expression and Purification. Variant cell lines H242A (kindly provided to us by R. E. Mains and B. A. Eipper) and H107AH108A (constructed in house) were grown as described previously.[9,13] Briefly, the stably transfected cell lines were thawed from a freezer stock in a T75 flask with 20 mL of DMEM/F12 medium containing 10% FCII serum (Fisher). At 80% confluence, the cells were passed into five NUNC triple flasks (500 cm^2 per flask) that were also grown to confluence. Cells were trypsinized and resuspended in 50 mL of medium with 10% FCII serum prior to being inoculated into the extracapillary space (ECS) of a Hollow Fiber Bioreactor (Fibercell Systems 4300-C2008, MWCO of 5000, 3000 cm^2 surface area) precultured first with 2 L of 50 mM PBS (pH 7.35) and then with 2 L of DMEM/F12 10% FCII serum.[9,13,19,25] Individual bioreactors containing each of the variants were fed with DMEM/F12/10% FCII serum for a month, after which the serum level was reduced to 0.5% FCII serum.[25] At this point, the bioreactors were fed with 0.5% serum-containing medium every other day, and spent medium (20 mL) from the ECS was collected and frozen at −20 °C for later purification. After being harvested in the bioreactor for a month (300 mL), each variant was purified as previously described.[25]

dx.doi.org/10.1021/bi4015264 | *Biochemistry* 2014, 53, 1069−1080

Reconstitution with Copper. Initially, the single-site variants were dialyzed against 20 mM sodium phosphate buffer (pH 8.0) overnight and then reconstituted with up to 2 equiv of cupric sulfate by slow addition (60 μL/h) followed by exhaustive dialysis. This procedure led to copper:protein ratios close to 1. Thereafter, the single-site mutants were reconstituted with 1.3 equiv of cupric sulfate, dialyzed overnight against 20 mM sodium phosphate buffer, concentrated using ultrafiltration, and passed through a desalting spin column to remove any remaining unbound cupric ions. The protein concentration was determined by OD_{280} on a Cary 50 UV−vis spectrophotometer at room temperature using an absorbance at 280 nm for a 0.1% solution (1 mg/mL in a 1 cm path length cell) of 0.980.[9] The copper concentrations were determined using a Perkin-Elmer Optima 2000 DV inductively coupled plasma optical emission spectrometer (ICPOES).

Reconstitution with Silver. All silver reconstitutions were conducted in a dark room, with the sample and the silver nitrate stock solutions (100 mM) covered by aluminum foil. Variants were exhaustively dialyzed against MES buffer (50 mM, pH 6.0) overnight, to exchange residual phosphate and chloride ions present in the buffer used for enzyme isolation. The protein was then reconstituted with 1.3 equiv of a freshly prepared $AgNO_3$ solution using a syringe pump at a rate of 30 μL/h. The reconstituted protein was gently stirred for 1 h and then passed through two MES buffer-equilibrated desalting columns. The M109I variant was reconstituted with 2.5 equiv of freshly prepared $AgNO_3$ at a pump rate of 30 μL/h followed by stirring for 1 h, and two cycles of desalting on MES buffer-equilibrated spin columns. Protein concentrations were determined as described for copper above. Silver concentrations were determined by ICPOES.

Activity Measurements. The enzymatic activities of H107AH108A and H242A were measured by monitoring oxygen consumption in a Rank Brothers oxygen electrode at 37 °C as previously reported.[16] The reaction was performed in a water-jacketed cell at 37 °C. The mixture (2 mL) contained 100 mM MES (pH 5.5), 200 μL of a 6 mg/mL catalase solution (~50000 units), a 5 μM copper sulfate solution, 10 mM ascorbate, and 80 μM dansyl-YVG substrate. The reaction mixture was allowed to equilibrate for several minutes, after which it was capped and a baseline was measured for 50 s. The reaction was then initiated by adding 10−30 μL of enzyme, through the cap of the reaction vessel with a 50 μL Hamilton syringe. The enzyme concentration for mutants was varied from 100 to 350 μM. Oxygen consumption was monitored and analyzed as previously reported.[16,19]

Collection and Analysis of EPR Spectra. Quantitative X-band (9.4 GHz) EPR spectra were recorded on a Bruker Elexsys E500 spectrometer equipped with a Bruker ER049X SuperX microwave bridge, and an E27H lock-in detector. Temperature control was provided by a continuous nitrogen flow cryostat system, in which the temperature was monitored with a Bruker W1100321 thermocouple probe. Frozen Cu(II) protein samples at concentrations between 100 and 500 μM in 50 mM MES buffer (pH 5.8, with no cryoprotectant) were measured in 4 mm silica tubes at 90−110 K under nonsaturating power conditions. EPR spectra were simulated using SIMPIP, developed at the University of Illinois (Urbana, IL) and described in detail elsewhere.[26]

Sample Preparation for XAS. The oxidized protein samples were prepared in a single step by 5-fold dilution of enzyme at a concentration of 4 mM in Cu(II) with either 50 mM sodium phosphate buffer (pH 7.5) or 50 mM MES and 50 mM formic acid (pH 5.5 or 3.5), as necessary. Ethylene glycol was added to a concentration of 20% of the total volume. Reduced protein samples were prepared under anaerobic conditions by 5-fold dilution with pH-adjusted anaerobic buffers to which 5 mM ascorbate had been added along with 20% ethylene glycol. Samples were transferred to XAS cuvettes and flash-frozen in liquid nitrogen. The final concentration of copper or silver varied from 600 to 1200 μM.

Collection and Analysis of XAS Data. Samples were measured as aqueous glasses in 20% ethylene glycol at 10 K. Copper K-edge (8.9 keV) and Ag K-edge (25.5 KeV) extended X-ray absorption fine structure (EXAFS) and X-ray absorption near edge structure (XANES) data were collected at the Stanford Synchrotron Radiation Lightsource operating at 3 GeV with currents close to 500 mA maintained by continuous top-off.

Cu K-edges were measured on beamline 9-3 using a Si[220] monochromator and a Rh-coated mirror upstream with a 12.5 keV energy cutoff to reject harmonics. Data were collected in fluorescence mode using a high-count rate Canberra 100-element Ge array detector with maximal count rates per array element of <120 kHz. A nickel oxide filter and Soller slit assembly inserted in front of the detector was used to reduce elastic scattering relative to the Cu Kα fluorescence. Four to six scans of a sample containing only buffer were averaged and subtracted from the averaged data for each protein sample to remove the Ni Kβ fluorescence and produce a flat pre-edge baseline.

Ag K-edge data (25.5 KeV) were measured on beamline 7.3 using nitrogen-filled ion chambers operating at 1.5 kV. The energy cutoff mirror (used for harmonic rejection) was removed to achieve the high energy, and the Si(220) monochromator was fully tuned to optimize incident counts. While the setup did not provide for harmonic rejection, the level of harmonic contamination at this energy was expected to be low. Energy calibration was achieved with a Ag foil placed between the second and third ionization chambers. The EXAFS was detected by Ag Kα fluorescence using a Canberra 30-element detector with count rates kept below 120 Hz per channel to avoid saturation. Soller slits and a Pd foil were used to attenuate the elastic scatter peak. Four to six scans of a sample containing only buffer were averaged and subtracted from the averaged data for each protein sample to remove the Pd Kβ fluorescence and produce a flat pre-edge baseline.

Data reduction and background subtractions were performed using the program modules of EXAFSPAK.[27] Output from each detector channel was inspected for glitches and dropouts before inclusion in the final average. Spectral simulation was conducted using EXCURVE version 9.2[28−30] as described previously.[13] Simulations of the EXAFS data used a mixed-shell model consisting of imidazole from histidine residues and S from methionine coordination. The threshold energy, E_0, was set at 8985 eV for Cu and 25520 eV for Ag. Refinement of structural parameters included distances (R), coordination numbers (N), and Debye−Waller factors ($2\sigma^2$) and included multiple scattering contributions from outer-shell atoms of imidazole rings and from linear CO groups.

CO Binding. Purified WT PHMcc, H107AH108A, and H242A were concentrated to approximately 4 mM Cu in 20 mM phosphate (pH 8.0). The pH was then adjusted by diluting the concentrated enzyme four times with 50 mM MES/HEPES/CHES/formate mixed buffer at pH 3.5 or 7.5 in a

dx.doi.org/10.1021/bi4015264 | Biochemistry 2014, 53, 1069−1080

septum-sealed conical vial. Samples were purged under a gentle stream of CO gas for 5 min before the addition of a 5-fold excess (5 mM) of anaerobic buffered ascorbate and then incubated under an atmosphere of pure CO for an additional 5 min.

Fourier Transform Infrared Spectroscopy. After reaction with CO, protein solutions were loaded into the IR cell (50 μm path length) at a final concentration of 1 mM in copper. After the protein data had been collected, the cell was flushed with buffer and a baseline was recorded. FTIR data were recorded on a Bruker Tensor 27 FTIR spectrometer at room temperature with a sample chamber that was continuously purged with dry CO_2-free air. Samples were equilibrated inside the instrument sample chamber for 15 min to allow purging of water vapor and CO_2 prior to data collection. One thousand scans were collected for each sample and buffer spectrum from 2200 to 1950 cm^{-1} at a nominal resolution of 2 cm^{-1}. Baseline subtraction and spectral analysis were performed using the GRAMS AI Spectroscopy Software (Thermo).

RESULTS AND DISCUSSION

Copper Binding Stoichiometry and Catalytic Activity. Each of the two single-site variants was tested for its capacity to bind copper. Apoproteins were incubated with up to 2 equiv of cupric sulfate added slowly by syringe pump, followed by exhaustive dialysis or desalting on at least two spin columns. For H242A, the stoichiometry of Cu(II) binding was 1.11 ± 0.03 (average of five measurements), while for H107AH108A, the stoichiometry was 1.09 ± 0.15 (average of six measurements). The catalytic activity of each variant was measured using the standard assay of oxygen uptake on an oxygen sensitive electrode where the slope of the O_2 concentration versus time plot is a direct measure of enzyme activity. Reactants (excluding the enzyme) were incubated together for several minutes prior to initiation by the enzyme. The slope of the oxygen concentration versus time curve did not change after initiation, even at high protein concentrations (up to 350 μM). This is in marked contrast to the case for the WT enzyme, which gives slopes approaching the diffusion limit of oxygen across the electrode membrane at enzyme concentrations of $\lesssim$30 μM. We conclude that neither variant has measurable catalytic activity, consistent with the hypothesis that each represents a single-site mutant, where the absence of the second copper atom completely abrogates catalytic activity.

Structural Properties of the Cu(II) Proteins. XAS and EPR spectra were recorded on the oxidized forms of H107AH108A and H242A variants to provide spectroscopic evidence of their formulation as single-site derivatives. Previous EXAFS data for the cupric form of the WT protein were consistent with ligand sets of $(His)_3(OH_2)$ and $(His)_2(OH_2)_2$ for H and M, respectively, where the S(Met) interaction at M is undetectable.[13,14] Also, EXAFS spectra of the oxidized forms of metal site His to Ala mutants such as H107A, H108A,[19] and M314H[16] were found to be extremely similar to those of WT and to each other, because the ligand sets differ by an average of 0.5 His ligand per copper. In the present case, the expectation is that single-site H and M spectra should likewise be similar, a prediction borne out by the nearly identical X-ray absorption near edge structure (XANES) (Figure 2a) of the two variants. Although the H-center should have one more histidine per Cu(II), the overall two-site equatorial coordination is consistently 4N/O. Any EXAFS difference should then be manifest only in the outer-shell signatures of imidazole ligation

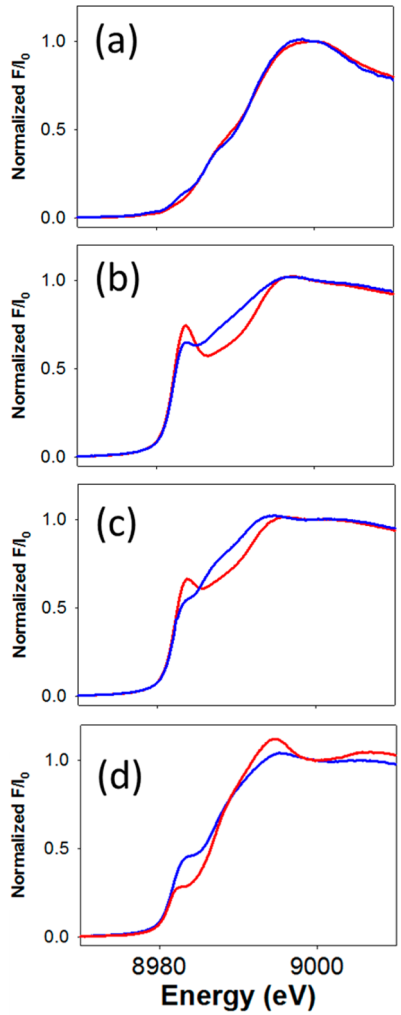

Figure 2. X-ray absorption edge spectra for PHM single-site variants. (a) Cu(II) spectra H107AH108A (red), H242A (blue). (b) Cu(I) spectrum of H-site variant H242A at pH 7 (red) and pH 3.5 (blue). (c) Cu(I) spectrum of M-site variant H107AH108A at pH 7 (red) and pH 3.5 (blue). (d) Spectra of Cu(I)−CO complexes of the M-site variant at pH 7 (red) and the H-site variant at pH 3.5 (blue). All edge spectra were normalized at 9000 eV.

in the Fourier transforms (FT) around 3 and 4 Å, respectively. Figure 3a compares the FTs of H242A and H107AH108A variants. In line with prediction, the intensity of the first shell is very similar, while a significant increase in the outer-shell amplitude is observed for the H242A H single site. Panels b and c of Figure 3 show simulations of the M-site [2N(His) + 2O(solvent)] and H-site [3N(His) + 1O(solvent)], respectively, with their metrical parameters listed in Table 1. The fits were obtained by constraining the Debye−Waller (DW) factors for the outer-shell imidazole atoms to be the same in each fit, while allowing the imidazole occupation number to increase from 2 (M-site) to 3 (H-site). The excellent agreement between theory and experiment for the outer-shell features is convincing evidence of the predicted ligand sets of H- and M-sites, respectively.

Figure 4 compares EPR spectra for the H242A and H107AH108A variants. The spectra show significant differences in the parallel region (Figure 4a), while simulations (Table 2 and Figure 4b,c) show that the origin of these differences is largely the difference in the value of $g_{\|}$ with the H-site single

dx.doi.org/10.1021/bi4015264 | Biochemistry 2014, 53, 1069−1080

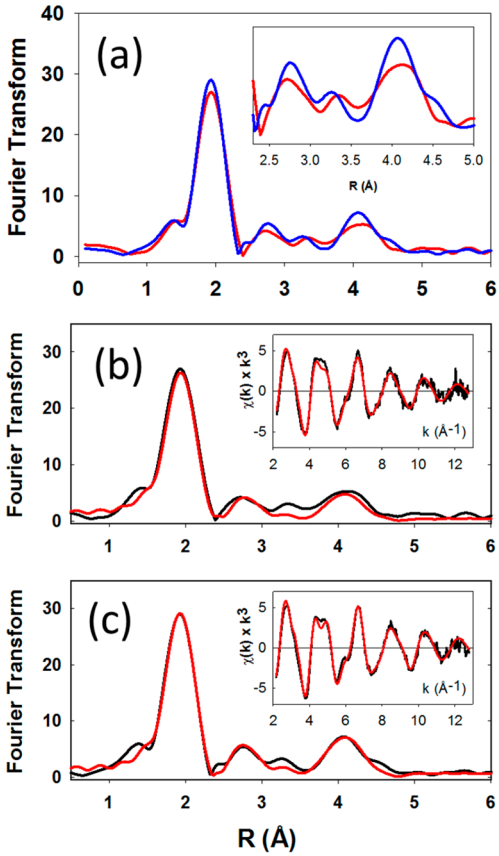

Figure 3. EXAFS spectroscopy of oxidized forms of PHM single-site variants. (a) Comparison of the experimental Fourier transforms of the M-site (H107AH108A, red) and H-site (H242A, blue). The inset shows an expanded view of the 2.5−5 Å region of the FT to indicate the difference in intensity between the M-site (red, two coordinated imidazoles) and the H-site (blue, three coordinated imidazoles). (b and c) Experimental (black) and simulated (red) FTs and EXAFS (insets) for the M-site (H107AH108A) and the H-site (H242A) single-site variants, respectively. Parameters used in these fits are listed in Table 1.

variant (H242A) having a lower value than the M-site single variant (H107AH108A). This is expected on the basis of Peisach−Blumberg correlations that predict that sites with more N donors have lower values of $g_{\|}$.[31] The effect of adding together the spectra of the two variants in equal (0.5) proportions and comparing the sum with the spectrum of the WT protein is shown in Figure 4d. The composite spectrum is a reasonable match to that of the WT protein as predicted if the EPR spectra of the individual sites are additive and the sites do not interact. The residual after subtraction of the composite spectrum from the WT is shown in Figure 4e, where the lack of any broad underlying signal again suggests that the two sites do not interact or that any interaction cannot be detected at the temperature of the measurement (170 K). On the other hand, the g and A values of the single-site variants correlate less well with the two-site simulation of the WT spectrum reported earlier and included in Table 2 for comparison.[19] It is unclear whether this discrepancy relates to inadequacies in the two-site fitting model or to perturbations in the single-site variants relative to the WT protein, but the good correspondence between WT and the 50:50 composite spectrum suggests the former. The bottom panel of Figure 4 shows expanded views of the parallel region for the spectra shown in parts a, d, and e of Figure 4.

Structural Properties of the Cu(I) Centers. The Cu(I) forms of the single-site variants were prepared by ascorbate reduction of their cupric forms. The structures and chemistry of the reduced sites are distinct and offer a more sensitive basis for assessing the fidelity of the single-site variants with respect to the native protein. Previous studies of WT PHM and a variety of H- and M-site variants have provided working assignments for spectral signatures characteristic of the H- and M-site Cu(I) centers. For example, on the basis of EXAFS and FTIR of unligated variants and their CO complexes conducted as a function of pH, $Cu_H(I)$ was predicted to be coordinated to two or three His residues at pH >6 in a configuration that did not bind CO, whereas a conformational switch to a His + S(Met) form was observed at pH <6, which now bound CO with a $\nu(C{\equiv}O)$ of 2110 cm^{-1}. $Cu_M(I)$ was coordinated by two His residues and a weakly bound S(Met) and bound CO at all pH values with a $\nu(C{\equiv}O)$ of 2092 cm^{-1}. All of these systems bound copper at both sites.[9,19] Therefore, while the spectral assignments were generally consistent with the available data, the uncertainties introduced by the presence of two chemically inequivalent Cu(I) centers led to ambiguity.

Figure 2b shows X-ray absorption edge data for the reduced H242A (H-site) variant at pH 7.5 (red) and pH 3.5 (blue). The absorption edges show significant differences. At pH 7.5, a relatively intense feature is observed at 8983.7 eV indicative of low-coordinate Cu(I)−bis-imidazole complexes[32−34] and suggesting that at neutral pH the H-center binds only two of the three available histidine ligands. Analysis of the EXAFS (Figure 5, top panel) confirms this conclusion where the metrical environment simulates to two imidazole ligands with a characteristically short Cu−N(imid) distance of 1.89 Å (Table 1).[32,33] These data present the intriguing result that one of the three His ligands is dissociated at neutral pH and imply that a significant conformational change occurs upon reduction. At a low pH (3.5), a different coordination is observed, depicted by a decrease in the 8983 eV intensity (Figure 2b, blue trace), and the attenuation of the Cu−N peak and the appearance of a new Cu−S interaction at ∼2.3 Å in the Fourier transform (Figure 5, bottom panel). These changes are similar to those reported earlier for the WT enzyme, absent in the M109A variant, and interpreted as a conformational switch induced by a protonation event that allows the noncoordinating M109 to flip into a coordinating position.[19] The Cu−S and Cu−N distances (Table 1) are now typical of three coordination, implying that the Cu(I) retains two His residues, but the Cu−N DW factor has increased, suggesting more disorder in the Cu(I)−histidine diad. The data do not indicate whether the protonating species is a H107 as previously suggested,[19] but the following scenario could account for the data. At neutral pH, the WT CuH binds H107 and H108 in a linear configuration with H172 dissociated; when the pH is lowered, H107 is protonated and induces a conformational change to a form involving a triad of H108, H172, and M109.

The DW value derived via simulation of the low-pH data using an N_2S ligand set requires comment. The DW is nearly twice that observed for the low-pH form of the WT protein, where contributions from both the H- and M-centers are averaged. As discussed above, our model for the low-pH transition at the H-center in WT PHM[19] involves protonation of one of the coordinating His residues, and replacement with the S ligand of the nearby M109 residue. Because the H-center

dx.doi.org/10.1021/bi4015264 | Biochemistry 2014, 53, 1069−1080

Table 1. Parameters Used To Fit the EXAFS Data for Oxidized and Reduced Forms of the M-Site (H107AH108A) and H-Site (H242A) Single-Site Variants of PHM

		Cu−N(His)[d]			Cu−O/N[e]			Cu−S			
	F[a]	No[b]	R (Å)[c]	DW (Å²)	No[b]	R (Å)[c]	DW (Å²)	No[b]	R (Å)[c]	DW (Å²)	$-E_0$
WT Protein[f]											
oxidized, pH 5.5	0.318	2.5	1.97	0.0123	1.5	1.97	0.0123				4.69
reduced, pH 7.5	0.373	2.5	1.92	0.0175				0.5	2.24	0.0123	0.34
reduced, pH 3.5	0.327	2.5	1.95	0.0182				1.0	2.26	0.0102	−0.66
M-Site (H107AH108A)											
oxidized, pH 5.5	0.324	2.0	1.98	0.012	1	1.98	0.012				4.59
reduced, pH 7.5	0.262	2.0	1.91	0.020				1	2.18	0.019	−0.36
reduced, pH 5.5	0.310	2.0	1.94	0.015				1	2.20	0.008	−0.36
reduced, pH 3.5	0.469	2.0	1.99	0.015				1	2.23	0.005	0.62
H-Site (H242A)											
oxidized, pH 7.0	0.223	3.0	1.97	0.010	1	1.97	0.10				4.85
reduced, pH 7.5	0.481	2.0	1.89	0.012							2.29
reduced, pH 3.5	0.454	2.0	1.92	0.026				1	2.25	0.007	−0.36

[a]F is a least-squares fitting parameter defined as $F^2 = (1/N)\sum_{i=1}^{N} k^6(\text{data} - \text{model})^2$. [b]Coordination numbers are generally considered accurate to ±25%. [c]In any one fit, the statistical error in bond lengths is ±0.005 Å. However, when errors due to imperfect background subtraction, phase shift calculations, and noise in the data are compounded, the actual error is closer to ±0.02 Å. [d]Fits modeled histidine coordination by an imidazole ring, which included single and multiple scattering contributions from the second-shell (C2/C5) and third-shell (C3/N4) atoms, respectively. The Cu−N−C_x angles were as follows: Cu−N−C2, 126°; Cu−N−C3, −126°; Cu−N−N4, 163°; Cu−N−C5, −163°. [e]Distances of the Cu−N(His) and Cu−N/O (non-His) shells were constrained to be equal in fits to the oxidized proteins. [f]Data from ref 19.

single-site variant appears to coordinate only two His residues at neutral pH, it is reasonable to ask whether the high DW reflects the fact that the low-pH form of the H242A variant is two- rather than three-coordinate, resulting from the protonation and replacement of one of these with M109. However, from simulations, neither the goodness of fit nor the values of the bond lengths support a two-coordinate structure, with the Cu−S distance well-defined at its three-coordinate value of 2.25 Å. We may conclude that the high DW must arise from an increased level of disorder in the site, perhaps as a result of multiple species present at equilibrium. One possibility is that the pK_a for the protonation event in the variant may be lower than its WT value (4.6),[16] leading to only partial conversion between the Met-off and Met-on forms. Alternatively, more than one His residue may be protonated, resulting in more complex speciation with fluxional Cu−His coordination. Thus, the ligand dynamics of the low-pH Cu(I)−N_2S site of the H-center [strong Cu−S(Met) with disordered Cu−His coordination] appear to be different from those of the M-center (*vide infra*) where the reverse appears to be true.

XAS data were also collected on the H107AH108A (M-site) variant and are shown in Figures 2c (edge data at pH 7.5 and 3.5) and 6 (EXAFS data at pH 7.5, 5.5, and 3.5). Absorption edges are generally typical of three-coordinate species. EXAFS analysis (Table 1) indicates the presence of two imidazole ligands and one methionine ligand as expected for the His_2Met ligand set with distances typical of this coordination environment. The surprising feature of these spectra is the variation in the intensity of the Cu−S(Met) interaction as the pH is lowered, where the simulations show a significant increase in DW factor with an increase in pH. One explanation of this behavior is that the M-center is comprised of two different conformers, a Met-on form (low pH) and a Met-off form (neutral pH) interconverting via a deprotonation event. The observed distances appear to validate this hypothesis. At neutral pH, both the Cu−N and Cu−S distances are short and suggestive of two coordination; therefore, it is reasonable to posit that the site is fluxional and interconverts between His-His and His-Met ligand pairs. At low pH, the distances become longer and become more characteristic of three coordination, with a marked decrease in the DW factor of the Cu−S(Met) interaction. We hypothesize that protonation of a non-coordinating residue removes some constraint on the configuration of the three copper-binding residues, allowing them to relax to a more stable conformational state.

The fluxional model predicts that an equivalent fit should be obtained using parameters that represent the average of the two interconverting conformers. We tested this prediction for both neutral and low-pH states using a model that allowed Cu−N and Cu−S shell occupancies to vary while keeping the overall coordination number fixed at 2. At pH 7, an adequate fit (F = 0.38 vs 0.26) could be obtained with 1.45 Cu−N(His) and 0.55 Cu−S(Met) at the same distances but with lower DW factors (Figure S1 of the Supporting Information, top panel). At low pH, however, simple averaging resulted in poorer simulations, but introduction of a substoichiometric Cu−N interaction at 1.87 Å led to a much improved fit (0.28 vs 0.47), particularly with respect to the low-R shoulder in Figure 6 (bottom panel) and with more reasonable DW factors of the Cu−N shells (Figure S1 of the Supporting Information, bottom panel). This may suggest the presence of both two-coordinate and three-coordinate conformers existing in equilibrium at low pH arising from more complex ligand dynamics.

Examination of the crystal structure suggests a plausible explanation for this behavior. The distance between the main chain amide N of the M-coordinating H244 and one of the carboxylate oxygens of E313 is 2.78 Å, which is in the range expected for a H-bond between these residues. E313 is part of the fully conserved $E^{313}M^{314}C^{315}$ triad. We note that protonation of the carboxylate side chain of E313 would sever this H-bond and remove the constraint on the position and conformation of H244 as well any constraint on E313's neighbor, the M314 copper ligand. The pH dependence of M-site S(met) coordination was not detected in our previous pH-dependent study of the WT protein,[16] largely because it was obscured by or averaged into the pH-dependent conforma-

dx.doi.org/10.1021/bi4015264 | *Biochemistry* 2014, 53, 1069−1080

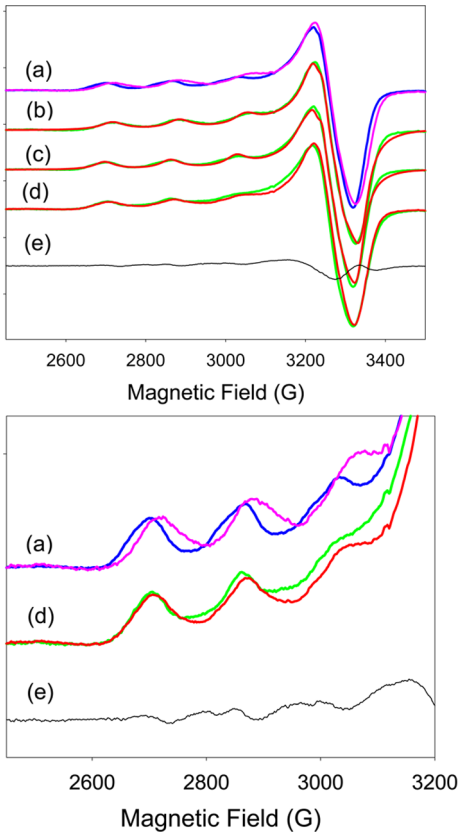

Figure 4. EPR spectra of M-site and H-site single-site variants. The top panel shows (a) a comparison of X-band spectra for the M-site (blue) and H-site (pink), (b and c) experimental (green) vs simulated (red) H-site (b) and M-site (c) spectra, (d) a comparison of composite spectra (50% H and 50% M, red) with the WT protein spectrum (green), and (e) the residual after subtracting the composite spectrum from the WT spectrum. EPR collection parameters were as follows: microwave frequency of 9.396 GHz, modulation amplitude of 4 G, microwave power of 2 mW, and temperature of 170 K. The *g* and *A* values are listed in Table 2. The bottom panel shows an expanded view of the parallel hyperfine region for spectra a, d, and e.

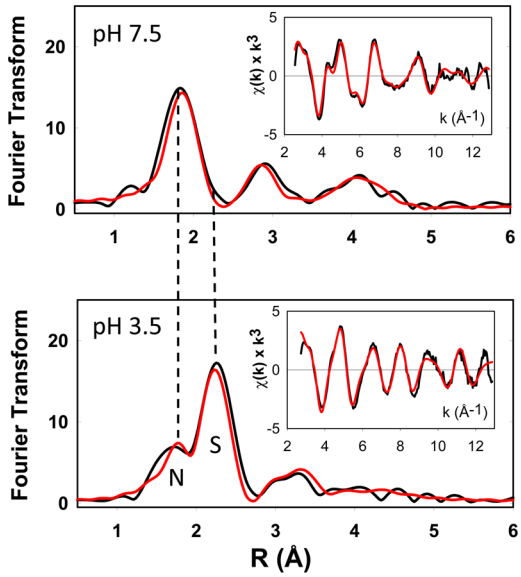

Figure 5. Experimental and simulated Fourier transforms and EXAFS (insets) for reduced Cu(I) forms of the H-site variant (H242A) at pH 7.5 (top) and pH 3.5 (bottom). Parameters used in the fits are listed in Table 1.

tional switch at the H-center, and it is therefore unclear whether the M-site undergoes the same pH-dependent change in the WT protein.

CO Complexes. We also investigated the CO binding properties of both single-site variants as a function of pH, using FTIR and XAS. Panels a and b of Figure 7 compare the FTIR in the 2200−1950 cm^{-1} region for the CO complexes of H242A (H-site) at pH 7.5 and 3.5. On the basis of previous assignments derived from measurements of the WT and M109A derivatives, an H-site single-site variant is predicted to bind no CO at neutral pH but forms a CO complex at low pH where the S donor atom from M109 enters the coordination sphere.[19] In line with these predictions, no ν(CO) is observed at pH 7.5, whereas a rather weak band centered at 2102 cm^{-1} is found at pH 3.5, blue-shifted relative to that of the WT protein by ∼8 cm^{-1}. The carbon−oxygen stretching frequency of Cu(I)−carbonyl complexes is a sensitive index of coordination and/or ligand conformation. ν(C≡O) is a measure of the C−O bond order, which is modulated by the degree of back-bonding from the filled d shell of Cu(I) into the empty π-antibonding orbitals on CO, and is further influenced by the donor power of the other ligands to Cu(I). These trends are illustrated by the frequency of carbonmonoxy hemocyanin [$Cu(His)_3$, 2043−2063 cm^{-1}] relative to PHM and DBM [$Cu(His)_2$(Met), 2089−2093 cm^{-1}], where substitution of the stronger histidine donor for the weaker thioether results in less back-bonding and a higher frequency for PHM/DBM.[9,14,35] However, CO frequencies are also highly sensitive to metal site electronic structure, conformational state, and site polarity. In *Thermus thermophilus*, ν(C≡O) for the Cu_B−CO photoproduct of the caa_3 oxidase is 10 cm^{-1} higher than that of the ba_3 Cu_B−CO photoproduct, even though the ligand set consists of three His residues in both cases,[36,37] which indicates at least two conformations in the Fe_{a3}−Cu_B active site cavity.[38] PHM and DBM likewise share identical ligand sets at CuM, but their ν(C≡O) values differ by 3 cm^{-1}; CO frequencies of hemocyanins from different species vary between 2043 and 2063 cm^{-1}.[39] The 8 cm^{-1} shift in ν(CO) for the H242A variant is therefore not inconsistent with the $Cu(His)_2S$(Met)CO

Table 2. Spin Hamiltonian Parameters Deduced from the Simulation of the EPR Spectra of M-Site (H107AH108A) and H-Site (H242A) Single-Site Variants of PHM[a]

	g_x	g_y	g_z	$A(x,y)$	$A(z)$	$W(x,y)$	$W(z)$
WT, site 1	2.051	2.069	2.300	18	533	49	106
WT, site 2	2.042	2.083	2.279	25	510	49	94
H107AH108A	2.045	2.071	2.280	17	526	53	103
H242A	2.043	2.070	2.263	24	527	55	118

[a]Hyperfine values are in megahertz.

dx.doi.org/10.1021/bi4015264 | *Biochemistry* 2014, 53, 1069−1080

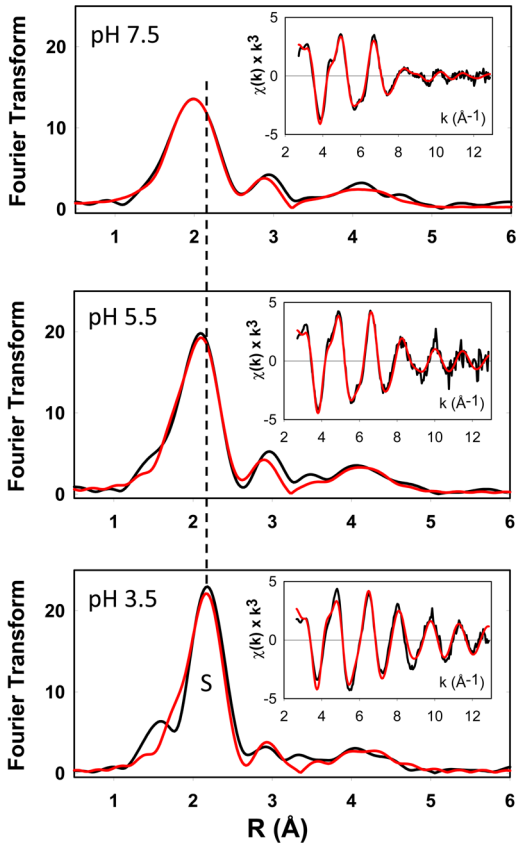

Figure 6. Experimental and simulated Fourier transforms and EXAFS (insets) for reduced Cu(I) forms of the M-site variant (H107AH108A) at pH 7.5 (top), 5.5 (middle), and 3.5 (bottom). Parameters used in the fits are listed in Table 1.

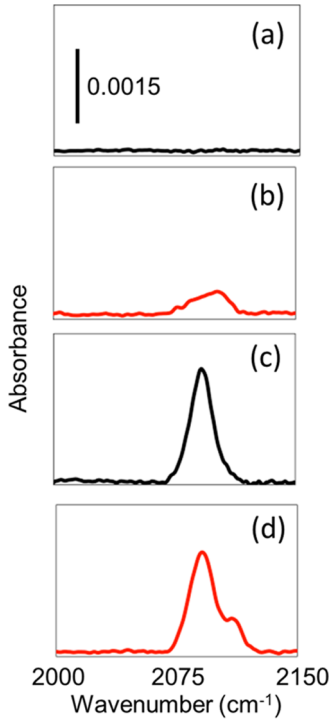

Figure 7. FTIR spectra of single-site Cu(I)−CO complexes: (a) H-site CO at pH 7.5, (b) H-site CO at pH 3.5, (c) M-site CO at pH 7.5, and (d) M-site CO at pH 3.5.

coordination proposed for the low-pH CO complex of the H-center in the WT protein, but the His-Met donor power, ligand conformation, or the site polarity must be different in the H single-site variant. It is also unclear why the intensity of the low-pH band is so much lower than that of the WT protein.

Panels c and d of Figure 7 compare the CO complexes of the H107AH108A (M-site) variant at pH 7.5 and 3.5. Both spectra show the intense 2092 cm^{-1} band previously assigned to the M-site carbonyl. These data provide an unambiguous assignment of the origin of this IR band. The arguments in the preceding paragraph relating small changes in ν(C≡O) to conformational variation among complexes of the same ligand set have a converse, namely, that invariant frequencies are indicators of highly similar coordination and conformation. The invariant ν(C≡O) of WT and H107AH108A carbonyls therefore establishes that the ligand set and conformation of the carbonyl are identical in WT and the M single-site variant. The low-pH spectrum also shows a small shoulder at 2111 cm^{-1}. This feature could be due to a small component of a different conformation because bands at a similar frequency (with a much higher intensity) were observed previously for a low-pH H-site CO complex of the WT enzyme, which was shown to have a similar ligand set due to low-pH-induced flipping of M109 (*vide supra*).[19] However, the structural differences between conformers and the factors that control their distribution are unknown at this time.

XAS was used to compare the structures of the H- and M-site carbonyls as shown in Figures 2d (XANES) and 8a,b (EXAFS).

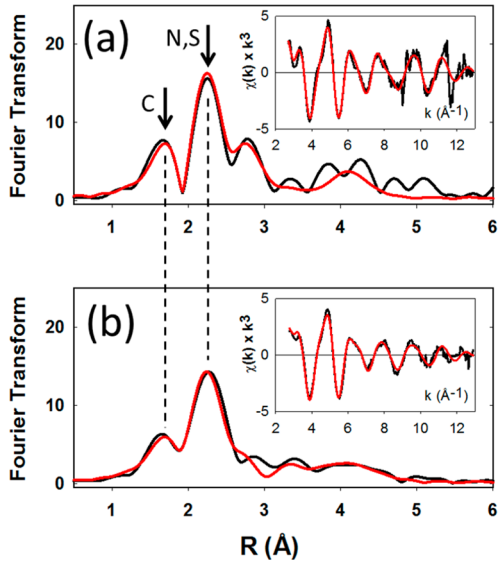

Figure 8. Experimental and simulated Fourier transforms and EXAFS (insets) for reduced Cu(I) forms of the single-site Cu(I)−CO complexes: (a) M-site CO at pH 7.5 and (b) H-site CO at pH 3.5. Parameters used in the fits are listed in Table 3.

Metrical parameters, including those of the coordinated CO derived from multiple scattering analysis, are listed in Table 3. The two carbonyls appear to be extremely similar with Cu−C and Cu−O distances of 1.80 and 2.85 Å and Cu−C−O angles of 171° and 179° for the H- and M-site complexes, respectively. From these values (and assuming errors in bond lengths of ±0.02 Å and angles of ±10°), the C−O bond distances calculate out as 1.05 ± 0.08 Å, which is consistent with the expected C−O distance of a coordinated carbonyl of ∼1.1 Å.

dx.doi.org/10.1021/bi4015264 | *Biochemistry* 2014, 53, 1069−1080

Table 3. FTIR Frequencies and EXAFS Fitting Parameters for the CO Complexes of M-Site (H107AH108A) and H-Site (H242A) Single-Site Variants of PHM

			Cu−N(His)[d]			Cu−C≡O[e]			Cu−S			
	ν(CO) (cm^{-1})	F[a]	No[b]	R (Å)[c]	DW (Å^2)	No[b]	R (Å)[c]	DW (Å^2)	No[b]	R (Å)[c]	DW (Å^2)	$-E_0$
M-Site (H107AH108A)												
pH 7.5	2092	0.74	2	1.97	0.023	1C	1.80	0.006	1	2.26	0.007	−0.92
						1O	2.85	0.024				
						∠Cu−C−O = 179°						
pH 3.5	2092					not determined						
H-Site (H242A)												
pH 7.5	none											
pH 3.5	2102	0.32	2	1.98	0.020	1C	1.81	0.009	1	2.27	0.009	−0.97
						1O	2.85	0.021				
						∠Cu−C−O = 170°						

[a] F is a least-squares fitting parameter defined as $F^2 = (1/N)\sum_{i=1}^{N} k^6(\text{data} - \text{model})^2$. [b] Coordination numbers are generally considered accurate to ±25%. [c] In any one fit, the statistical error in bond lengths is ±0.005 Å. However, when errors due to imperfect background subtraction, phase shift calculations, and noise in the data are compounded, the actual error is closer to ±0.02 Å. [d] Fits modeled histidine coordination by an imidazole ring, which included single and multiple scattering contributions from the second-shell (C2/C5) and third-shell (C3/N4) atoms, respectively. The Cu−N−C_x angles were as follows: Cu−N−C2, 126°; Cu−N−C3, −126°; Cu−N−N4, 163°; Cu−N−C5, −163°. [e] Metrical parameters for the CO ligand were simulated using full multiple scattering treatment. Cu−C and Cu−O distances and Cu−C−O angles were allowed to float in the fits.

Other details of the complexes reveal essentially identical ligand sets of two His residues, one S, and one CO, all with comparable and chemically reasonable distances and Debye−Waller factors. These structures are consistent with our predictions based on previous studies of the WT and its CO complexes. However, the M-site CO EXAFS data measured at pH 7.5 are of further interest because they establish that the Met ligand is fully coordinated to Cu(I) in the carbonyl (fully Met-on), even though M314 exists in Met-on and Met-off conformations in the unligated M-site at neutral pH. In this regard, the M-site CO structure corresponds to the Met-on conformation of the unligated M-site at pH 3.5, suggesting that CO binding provides a greater driving force than H-bonding (*vide supra*) in M-site conformational organization. This observation also rationalizes the invariant 2092 cm^{-1} frequency of the M−CO complex over the full pH range.

Silver Binding. We used single-site mutant H107AH108A to test whether other metals such as Ag(I) could bind at the M-center. When the M-site variant was reacted with an excess (1.3) of molar equivalents of silver nitrate in MES buffer (pH 6.0), followed by two rounds of desalting on MES buffer-equilibrated spin columns, the protein bound 1.06 ± 0.15 Ag(I) per protein, indicating tight binding of silver. This result was then used to examine whether the WT protein would similarly bind silver and whether the binding was selective for the M-site. Ag(I) is electronically homologous to Cu(I) and in general shows similar coordination chemistry,[40] although Ag is expected to have a higher affinity for ligand sets with S donors. Therefore, we used the M109I variant of the WT protein to control against M109 flipping that occurs at low pH and could influence Ag(I) binding at the H-center. The M109I variant (containing intact M- and H-sites) was incubated with 2.3 equiv of silver nitrate followed by two desalting steps and the silver content measured by ICPOES. The protein was found to bind 0.84 ± 0.11 Ag(I) per protein. Taken together, the results of these experiments imply that Ag(I) binds selectively at the M-center and has little or no affinity for the H-center. [Note that the analogous experiment of reacting Ag(I) with the H-site variant H242A was deemed unreliable as deletion of a single histidine may not be sufficient to abrogate binding of silver to the remaining His and Met at the M-site.]

The ligand environments of the silver complexes of H107AH108A and M109I were investigated by EXAFS measurements at the silver absorption edge. The high energy of the Ag K-edge makes these experiments challenging because of the low intensity and beam heterogeneity at the large monochromator angles necessary to reach the required energy (25.5 keV). These factors restricted the usable k range of the data to ≤11 Å^{-1}. EXAFS data for the M109I variant are shown in Figure 9. Simulation of the data requires the presence of both

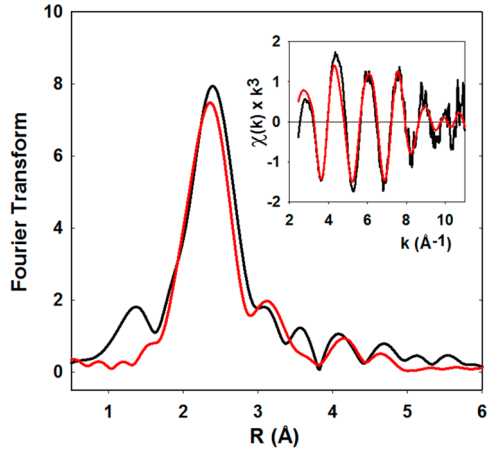

Figure 9. Experimental and simulated Fourier transform and EXAFS (inset) for the 1:1 Ag(I) complex of the M109I derivative of WT PHM. Data were collected at the Ag K-edge (25515 eV) and simulated with one Ag−N(His) component at 2.18 Å and one Ag−S component at 2.47 Å. Calculations included multiple scattering contributions from the histidine ligand using geometric parameters as listed for the copper EXAFS spectra in Table 1.

Ag−N and Ag−S components, but because both components have very similar phases, they are correlated given the restricted data range in k space. Notwithstanding, a good fit was obtained with one Ag−N(His) component at 2.2 Å and one Ag−S component at 2.5 Å, although alternatives of similar quality could be obtained varying the N- and S-shell occupancies but keeping their sum equal to 2. These results are similar to those obtained for the Cu(I) complex of H107AH108A at neutral pH

dx.doi.org/10.1021/bi4015264 | *Biochemistry* 2014, 53, 1069−1080

and validate the conclusion that silver binds exclusively at the M-center. EXAFS data for the Ag(I) complex of H107AH108A were of poorer quality (data not shown) but could be simulated by a N + S ligand set. However, the poorer data coupled to the correlation discussed above led to large uncertainties in both distances and coordination numbers, and the simulations are considered unreliable.

CONCLUSIONS

We have prepared and characterized two variants of PHM that contain mutations in the metal binding ligands at each of the two Cu centers. These derivatives bind only a single copper atom, suggesting that they indeed correspond to enzyme states with each of the two copper sites singly occupied. The variants are completely devoid of catalytic activity, emphasizing the obligatory requirement for both copper centers in the catalytic mechanism. The H242A variant contains copper only in the H-center, while the H107AH108A variant contains copper only in the M-center.

Detailed spectroscopic studies of the Cu(II) and Cu(I) forms of these derivatives provide robust assignments for spectral features previously observed in the WT protein. In particular, the unique chemistry of the M-center, including its His_2S(Met) ligation, and reactivity toward CO generating a carbonyl complex with ν(CO)=2092 cm^{-1} are faithfully reproduced in the H107AH108A variant. Likewise, the low-pH conformational switch described previously for the H-center[19] is also observed in the H242A variant. However, the study also uncovers new structural elements of both sites in the cuprous forms, which were previously obscured by spectral overlap between the two inequivalent coppers of the WT protein. For example, the H-center coordinates only two of its three His ligands in the Cu(I) state, while the M-site appears to undergo interesting pH-dependent conformational dynamics between Met-on (low-pH) and Met-off (neutral pH) forms. These new observations provide unique and critical insight into the catalytic roles of each copper center.

Ag(I) is iso-electronic with Cu(I) and has been shown to be handled by similar cellular transport processes.[41] Although complexes of Ag in the Ag(III) state exists, the instability of the Ag(II) state renders the metal unsuitable for a functional substitute for copper in enzymes such as PHM and DBM. However, substitution of one of the metal centers with Ag(I) would create heterobimetallic complexes in which the spectroscopy of the two centers does not overlap, allowing the structural elements of each site to be studied independently. Such studies would be a useful adjunct to single-site variants, as the effect of M-site metal occupancy on the structure of the H-site (and vice versa) could be distinguished. With this in mind, we used the H107AH108A variant to find conditions under which the Ag(I) ion could be incorporated at the PHM center and followed up with studies of Ag(I) with a WT analogue that showed that Ag(I) bound selectively at the M-center to generate a complex that gave structural (EXAFS) parameters similar to those of the Cu(I) complex. These data open the door to further investigations of the individual chemistry and spectroscopy of the metal centers in PHM. Although more challenging, the preparation of Ag/Cu heterobimetallic complexes is underway, and their detailed analysis will be the subject of future studies from this laboratory.

ASSOCIATED CONTENT

Supporting Information

Forward and reverse oligos used in the construction of H-site PHM single-site variant (Table S1) and alternate fits to the EXAFS of the reduced Cu(I) forms of the M-site single-site variant H107AH108A (Figure S1). This material is available free of charge via the Internet at http://pubs.acs.org.

AUTHOR INFORMATION

Corresponding Author

*E-mail: ninian@comcast.net. Phone: (503) 346-3428. Fax: (503) 346-3427.

Funding

This work was supported by a grant from the National Institutes of Health (R01 NS027583) to N.J.B. We gratefully acknowledge the use of facilities at the Stanford Synchrotron Radiation Lightsource, which is supported by the National Institutes of Health Biomedical Research and Technology Program Division of Research Resources and by the U.S. Department of Energy Office of Biological and Environmental Research.

Notes

The authors declare no competing financial interest.

ACKNOWLEDGMENTS

We thank Drs. Betty Eipper and Richard Mains for the gift of cell lines for the WT and H242A PHM proteins.

ABBREVIATIONS

CHES, *N*-cyclohexyl-2-aminoethanesulfonic acid; CHO, Chinese hamster ovary; dansyl-YVG, dansyl-Tyr-Val-Gly; DBM, dopamine β-monooxygenase; Dhfr, dihydrofolate reductase gene; DMEM F-12, Dulbecco's modified Eagle's medium; DW, Debye−Waller term; ECS, extra capillary space; EXAFS, extended X-ray absorption fine structure; FBS FCII, fetal clone II; FTIR, Fourier transform infrared; HEPES, 4-(2-hydroxyethyl)-1-piperazineethanesulfonic acid; ICP-OES, inductively coupled plasma optical emission spectrometry; MES, 2-(*N*-morpholino)ethanesulfonic acid; MWCO, molecular weight cutoff; PBS, phosphate-buffered saline; PHM, peptidylglycine monooxygenase; PHMcc, peptidylglycine monooxygenase catalytic core, residues 42−356; SDS−PAGE, sodium dodecyl sulfate−polyacrylamide gel electrophoresis; TBM, tyramine β-monooxygenase; WT, wild-type; XANES, X-ray absorption near edge structure; XAS, X-ray absorption spectroscopy.

REFERENCES

(1) Prigge, S. T., Mains, R. E., Eipper, B. A., and Amzel, L. M. (2000) New insights into copper monooxygenases and peptide amidation: Structure, mechanism and function. *Cell. Mol. Life Sci. 57*, 1236−1259.

(2) Chufan, E. E., Prigge, S. T., Siebert, X., Eipper, B. A., Mains, R. E., and Amzel, L. M. (2010) Differential reactivity between two copper sites in peptidylglycine α-hydroxylating monooxygenase. *J. Am. Chem. Soc. 132*, 15565−15572.

(3) Prigge, S. T., Eipper, B. A., Mains, R. E., and Amzel, M. (2004) Dioxygen binds end-on to mononuclear copper in a precatalytic enzyme complex. *Science 304*, 864−867.

(4) Prigge, S. T., Kolhekar, A. S., Eipper, B. A., Mains, R. E., and Amzel, L. M. (1997) Amidation of bioactive peptides: The structure of peptidylglycine α-hydroxylating monooxygenase. *Science 278*, 1300−1305.

(5) Prigge, S. T., Kolhekar, A. S., Eipper, B. A., Mains, R. E., and Amzel, L. M. (1999) Substrate-mediated electron transfer in peptidylglycine α-hydroxylating monooxygenase. *Nat. Struct. Biol. 6*, 976−983.
(6) Rudzka, K., Moreno, D. M., Eipper, B., Mains, R., Estrin, D. A., and Amzel, L. M. (2013) Coordination of peroxide to the Cu(M) center of peptidylglycine α-hydroxylating monooxygenase (PHM): Structural and computational study. *JBIC, J. Biol. Inorg. Chem. 18*, 223−232.
(7) Cardenas, D. J., Cuerva, J. M., Alias, M., Bunuel, E., and Campana, A. G. (2011) Water-based hydrogen-atom wires as mediators in long-range proton-coupled electron transfer in enzymes: A new twist on water reactivity. *Chemistry 17*, 8318−8323.
(8) Evans, J. P., Ahn, K., and Klinman, J. P. (2003) Evidence that dioxygen and substrate activation are tightly coupled in dopamine β-monooxygenase: Implications for oxygen activation. *J. Biol. Chem. 278*, 49691−49698.
(9) Jaron, S., and Blackburn, N. J. (1999) Does superoxide channel between the copper centers in peptidylglycine monooxygenase? A new mechanism based on carbon monoxide reactivity. *Biochemistry 38*, 15086−15096.
(10) Osborne, R. L., Zhu, H., Iavarone, A. T., Blackburn, N. J., and Klinman, J. P. (2013) Interdomain Long-Range Electron Transfer Becomes Rate-Limiting in the Y216A Variant of Tyramine β-Monooxygenase. *Biochemistry 52*, 1179−1191.
(11) Chen, P., and Solomon, E. I. (2004) O_2 activation by binuclear Cu sites: Noncoupled versus exchange coupled reaction mechanisms. *Proc. Natl. Acad. Sci. U.S.A. 101*, 13105−13110.
(12) Tano, T., Okubo, Y., Kunishita, A., Kubo, M., Sugimoto, H., Fujieda, N., Ogura, T., and Itoh, S. (2013) Redox properties of a mononuclear copper(II)-superoxide complex. *Inorg. Chem. 52*, 10431−10437.
(13) Blackburn, N. J., Rhames, F. C., Ralle, M., and Jaron, S. (2000) Major changes in copper coordination accompany reduction of peptidylglycine monooxygenase. *JBIC, J. Biol. Inorg. Chem. 5*, 341−353.
(14) Boswell, J. S., Reedy, B. J., Kulathila, R., Merkler, D. J., and Blackburn, N. J. (1996) Structural investigations on the coordination environment of the active-site copper centers of recombinant bifunctional peptidylglycine α-amidating enzyme. *Biochemistry 35*, 12241−12250.
(15) Chen, P., Bell, J., Eipper, B. A., and Solomon, E. I. (2004) Oxygen activation by the noncoupled binuclear copper site in peptidylglycine α-hydroxylating monooxygenase. Spectroscopic definition of the resting sites and the putative $CuII_M$-OOH intermediate. *Biochemistry 43*, 5735−5747.
(16) Bauman, A. T., Broers, B. A., Kline, C. D., and Blackburn, N. J. (2011) A Copper-Methionine Interaction Controls the pH-Dependent Activation of Peptidylglycine Monooxygenase. *Biochemistry 50*, 10819−10828.
(17) Hess, C. R., Klinman, J. P., and Blackburn, N. J. (2010) The copper centers of tyramine β-monooxygenase and its catalytic-site methionine variants: An X-ray absorption study. *JBIC, J. Biol. Inorg. Chem. 15*, 1195−1207.
(18) Jaron, S., Mains, R. E., Eipper, B. A., and Blackburn, N. J. (2002) The catalytic role of the copper ligand H172 of peptidylglycine α-hydroxylating monooxygenase (PHM): A spectroscopic study of the H172A mutant. *Biochemistry 41*, 13274−13282.
(19) Kline, C. D., Mayfield, M., and Blackburn, N. J. (2013) HHM motif at the CuH-site of peptidylglycine monooxygenase is a pH-dependent conformational switch. *Biochemistry 52*, 2586−2596.
(20) Eipper, B. A., Quon, A. S. W., Mains, R. E., Boswell, J. S., and Blackburn, N. J. (1995) The catalytic core of peptidylglycine α-hydroxylating monooxygenase: Investigation by site-directed mutagenesis, Cu X-ray absorption spectroscopy, and electron paramagnetic resonance. *Biochemistry 34*, 2857−2865.
(21) Kolhekar, A. S., Keutman, H. T., Mains, R. E., Quon, A. S. W., and Eipper, B. A. (1997) Peptidylglycine α-hydroxylating monooxygenase: Active site residues, disulfide linkages, and a two-domain model of the catalituc core. *Biochemistry 36*, 10901−10909.
(22) Horton, R. M., Cai, Z. L., Ho, S. N., and Pease, L. R. (1990) Gene splicing by overlap extension: Tailor-made genes using the polymerase chain reaction. *BioTechniques 8*, 528−535.
(23) Oyarce, A. M., Steveson, T. C., Jin, L., and Eipper, B. A. (2001) Dopamine β-monooxygenase signal/anchor sequence alters trafficking of peptidylglycine α-hydroxylating monooxygenase. *J. Biol. Chem. 276*, 33265−33272.
(24) Husten, E. J., and Eipper, B. A. (1991) The membrane-bound bifunctional peptidylglycine α-amidating monooxygenase protein. Exploration of its domain structure through limited proteolysis. *J. Biol. Chem. 266*, 17004−17010.
(25) Bauman, A. T., Ralle, M., and Blackburn, N. (2007) Large scale production of the copper enzyme peptidylglycine monooxygenase using an automated bioreactor. *Protein Expression Purif. 51*, 34−38.
(26) Nilges, M. J., Matteson, K., and Belford, R. L. (2006) A software package for the simulation of ESR powder-type spectra. In *ESR Spectroscopy in Membrane Biophysics* (Hemminga, M. A., and Berliner, L. J., Eds.) Springer, New York.
(27) George, G. N. (1995) *EXAFSPAK*, Stanford Synchrotron Radiation Laboratory, Menlo Park, CA.
(28) Binsted, N., and Hasnain, S. S. (1996) State of the art analysis of whole X-ray absorption spectra. *J. Synchrotron Radiat. 3*, 185−196.
(29) Gurman, S. J., Binsted, N., and Ross, I. (1984) A rapid, exact, curved-wave theory for EXAFS calculations. *J. Phys. C: Solid State Phys. 17*, 143−151.
(30) Gurman, S. J., Binsted, N., and Ross, I. (1986) A rapid, exact, curved-wave theory for EXAFS calculations. II. The multiple-scattering contributions. *J. Phys. C: Solid State Phys. 19*, 1845−1861.
(31) Peisach, J., and Blumberg, W. E. (1974) Structural implications derived from the analysis of electron paramagnetic resonance spectra of natural and artificial copper proteins. *Arch. Biochem. Biophys. 165*, 691−708.
(32) Himes, R. A., Park, G. Y., Siluvai, G. S., Blackburn, N. J., and Karlin, K. D. (2008) Structural studies of copper(I) complexes of amyloid-β peptide fragments: Formation of two-coordinate bis-(histidine) complexes. *Angew. Chem., Int. Ed. 47*, 9084−9087.
(33) Himes, R. A., Park, Y. G., Barry, A. N., Blackburn, N. J., and Karlin, K. D. (2007) Synthesis and X-ray absorption spectroscopy structural studies of Cu(I) complexes of histidylhistidine peptides: The predominance of linear 2-coordinate geometry. *J. Am. Chem. Soc. 129*, 5352−5353.
(34) Kau, L. S., Spira-Solomon, D. J., Penner-Hahn, J. E., Hodgson, K. O., and Solomon, E. I. (1987) X-ray absorption edge determination of the oxidation state and coordination number of copper: Application to the type 3 site in *Rhus vernicifera* laccase and its reaction with oxygen. *J. Am. Chem. Soc. 109*, 6433−6442.
(35) Pettingill, T. M., Strange, R. W., and Blackburn, N. J. (1991) Carbonmonoxy dopamine-b-hydroxylase: Structural characterization by FTIR, fluorescence and XAS spectroscopy. *J. Biol. Chem. 266*, 16996−17003.
(36) Einarsdottir, O., Killough, P. M., Fee, J. A., and Woodruff, W. H. (1989) An infrared study of the binding and photodissociation of carbon monoxide in cytochrome ba3 from *Thermus thermophilus*. *J. Biol. Chem. 264*, 2405−2408.
(37) Pinakoulaki, E., Soulimane, T., and Varotsis, C. (2002) Fourier transform infrared (FTIR) and step-scan time-resolved FTIR spectroscopies reveal a unique active site in cytochrome caa3 oxidase from *Thermus thermophilus*. *J. Biol. Chem. 277*, 32867−32874.
(38) Pavlou, A., Soulimane, T., and Pinakoulaki, E. (2011) Evidence for the presence of two conformations of the heme a3-Cu(B) pocket of cytochrome caa3 from *Thermus thermophilus*. *J. Phys. Chem. B 115*, 11455−11461.
(39) Fager, L. Y., and Alben, J. O. (1972) Structure of the carbon monoxide binding site of hemocyanins studied by Fourier transform infrared spectroscopy. *Biochemistry 11*, 4786−4792.
(40) Loftin, I. R., Franke, S., Blackburn, N. J., and McEvoy, M. M. (2007) Unusual Cu(I)/Ag(I) coordination of *Escherichia coli* CusF as revealed by atomic resolution crystallography and X-ray absorption spectroscopy. *Protein Sci. 16*, 2287−2293.

(41) Mealman, T. D., Blackburn, N. J., and McEvoy, M. M. (2012) Metal Export by CusCFBA, the Periplasmic Cu(I)/Ag(I) Transport System of *Escherichia coli*. *Curr. Top. Membr. 69*, 163−196.